Alexandria Engineering Journal (2020) 59, 3419–3429

HOSTED BY

Alexandria University

Alexandria Engineering Journal

www.elsevier.com/locate/aej
www.sciencedirect.com

A mathematical analysis of an isothermal tube drawing process

A.I.K. Butt [a], M. Abbas [a,b], W. Ahmad [a,*]

[a] Department of Mathematics, GC University, Lahore 54000, Pakistan
[b] Department of Mathematics and Applied Mathematics, University of Pretoria, Hatfield Campus, Pretoria, South Africa

Received 14 November 2019; revised 18 March 2020; accepted 19 May 2020
Available online 2 July 2020

KEYWORDS

Glass tube drawing process;
Existence and uniqueness;
Linear stability analysis;
Eigenvalue problem;
Critical draw ratio

Abstract The aim of this paper is to investigate stability of an isothermal glass tube drawing process through control parameters by the method of linear stability analysis. We want to see how the process parameters effect stability of the physical system being considered. For this purpose, we not only prove the existence and uniqueness of the solutions of steady state isothermal tube drawing model but also determine its numerical solution. To perform linear stability analysis, steady state numerical solution is incorporated in the eigenvalue problem, formulated by linearizing the isothermal model. The eigenvalue problem is then solved numerically to determine the critical draw ratio which indicates the onset of instabilities. To the end, stability of the process is analyzed using three different values of space step size. We also observe and discuss the effect of density, viscosity and pressure on stability of the isothermal tube drawing model.

1. Introduction

Glass tubes are manufactured through several continuous drawing processes to achieve the correct wall thickness and diameter. The most commonly used are the Danner and Vello processes [1–4] having great importance in glass fabricating industry for the continuous production of glass tubes and are still in use today. In Danner process, a glass is melted in a furnace to the stage when it becomes soft and pliable. Molten glass is then allowed to fall with low feeding speed v_0 on the surface of a cylindrical device called mandrel which is a slightly inclined hollow device such that the air can be blown through it. The mandrel is rotating about its axis of symmetry and is kept in a temperature controlled tank, called oven. By the continuous rotation of mandrel, molten glass falling downward creates a smooth layer around the mandrel. It cools down gradually and takes the shape of a thick-walled hollow glass tube with desired properties of design given at the end of a mandrel. We take the length of hot-forming zone equal to L. Glass tube is then pulled out by a drawing machine with a drawing speed $v_L > v_0$. The ratio $v_L/v_0 > 1$ is called the draw ratio. The drawn tube is then conveyed straight by rollers to further process of cutting, finishing, polishing and packaging at the end of the spinline. Keeping a constant temperature in the hot-forming zone leads to develop an isothermal glass tube drawing model. This manufacturing process is illustrated by the Fig. 1. The shaping parameters such as the wall thickness and cross-sectional area (or diameter) are the main characterizations of the drawn tube. In either of the manufacturing

* Corresponding author.
E-mail address: azhar.butt@gcu.edu.pk (A.I.K. Butt).
Peer review under responsibility of Faculty of Engineering, Alexandria University.

https://doi.org/10.1016/j.aej.2020.05.021

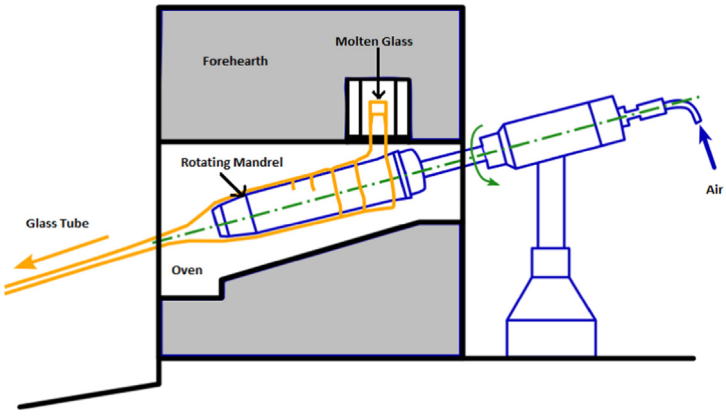

Fig. 1 Danner draw process.

processes, the required shape of the tube can be maintained by the stream of the air gently blown through the mandrel. Insufficient quantity of the air blown through the mandrel can disturb the desired shape of the glass tube. As a result, this insufficient balance collapse the walls of the glass tube. Moreover, the geometry of the glass tube can be controlled by the parameters involved herein such as the glass temperature, the composition of the raw material, the pressure of the blowing air in the mandrel and the rate of draw. It is to be remarkable that as compared to the other variables, the shaping parameters are significantly affected by the drawing speed which is considered as a control variable to control the geometrical aspects of the glass tube.

In glass industry, people are trying to control the geometry of the glass tube optimally and investigated the proper external parameters on their behalf through different techniques which have been discussed in literature [1,2,4–16,42]. Their goal is to control the circular, rectangular, square or triangular cross-sectional area of the tube drawn during the drawing process. In the recent past, a review on advances in metal micro-tube forming is given by Christoph Hartl [17]. A review on cold drawing process is performed by [18]. Some people worked for investigation on the residual stress state of drawn tubes by numerical simulation and neutron diffraction analysis [19]. A numerical simulation approach was used in [20] to estimate the most suitable input feedstock dimensions along with optimum plug-die position for production of multi-rifled tubes with given dimensions. To the best of our knowledge, the stability of the tube drawing processes has not yet been investigated and analyzed. We avail this opportunity.

Linear stability analysis is the most common and successful technique available in literature to analyze the stability of physical models. Basically, the linear stability follows the development, e.g. growth, oscillations or suppression of arbitrary small induced perturbations to understand the flow dynamics experimentally. For many years, the linear stability of system of differential equations is investigated and a significant number of important results have already been found regarding the stability of different physical processes. For example, this technique has been used to analyze the stability of fiber fabricating process by different researchers, we refer the readers to [21–29]. The stability of a melt spinning process with respect to some external parameters has been investigated in [30,31] by the method of linear stability analysis.

In this paper, we employ linear stability analysis approach to analyze the stability behaviour of an isothermal tube drawing process governed by a system of three coupled nonlinear partial differential equations. We linearize the system and formulate an eigenvalue problem. This problem is then solved numerically to determine the critical draw ratio in order to discuss the stability of tube drawing process. For the isothermal tube drawing, the system behaves an oscillatory instability when the draw ratio is greater than a critical draw ratio. It is observed that critical draw ratio decreases negligibly with the decrease in step size. Critically, we have observed that stability of an isothermal tube drawing model is affected by the density and viscosity of material and remains unchanged with the change in inside air pressure.

The structure of the paper is as follows: In Section 2, a mathematical model of the isothermal tube drawing process is explained. Section 3 deals with the steady state model. Existence and uniqueness of the solutions of steady state model is shown in Section 4. A numerical strategy to find the steady state solution of the model is studied in Section 5. Linear stability analysis for the isothermal case and the numerical implementation of results for the proposed problem is presented and discussed in Section 6. Section 7 contains the conclusion of our investigations.

2. Modeling isothermal tube drawing process

In the literature, different types of models for the drawing processes with different level of demands and descriptions are available. A considerable amount of work has been carried out by different researchers [1–3,32–39] to model the tube drawing process. In this section, we explain the mathematical model for an isothermal tube drawing process.

To model the tube drawing process, we consider an incompressible Newtonian flow of a molten glass between two free surfaces $r = r_1(z,t)$ and $r = r_2(z,t)$ where $r_1(z,t)$ and $r_2(z,t)$ respectively denote the inner and outer radii of the glass tube, and assume that temperature remains constant throughout the forming zone. Glass tube during production process is illustrated in Fig. 2. In the draw-down zone, the surface tension force and the inertial force acting upon the molten glass are insignificant and hence can be neglected. This kind of flow is governed by the equations

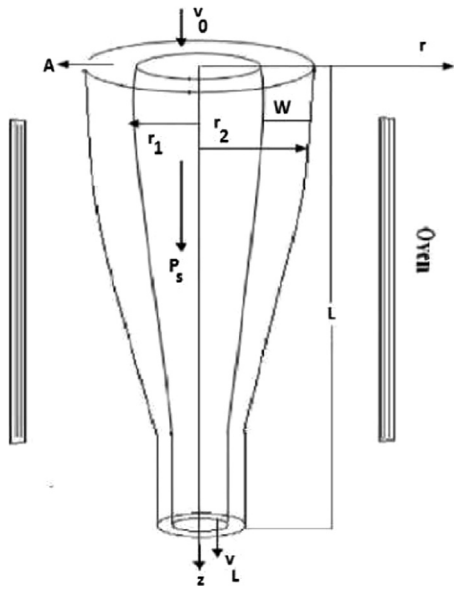

Fig. 2 Glass tube during production process.

$$\frac{\partial u}{\partial z}+\frac{1}{r}\frac{\partial}{\partial r}(rv)=0, \tag{2.1a}$$

$$\frac{\partial p}{\partial r}=\frac{\partial}{\partial z}\left(\mu\frac{\partial v}{\partial z}\right)+\mu\left(\frac{\partial^2 v}{\partial r^2}+\frac{1}{r}\frac{\partial v}{\partial r}-\frac{v}{r^2}\right)+2\frac{\partial \mu}{\partial r}\frac{\partial v}{\partial r}+\frac{\partial \mu}{\partial z}\frac{\partial u}{\partial r}, \tag{2.1b}$$

$$\frac{\partial p}{\partial z}=\frac{1}{r}\frac{\partial}{\partial r}\left(\mu r\frac{\partial v}{\partial z}\right)+\frac{1}{r}\frac{\partial}{\partial r}\left(\mu r\frac{\partial u}{\partial r}\right)+\rho g+\frac{\partial}{\partial z}\left(2\mu\frac{\partial u}{\partial z}\right). \tag{2.1c}$$

The Eqs. (2.1a)-(2.1c) are taken from [3] and are known as the standard equations showing the axi-symmetric stokes flow. The first equation is the continuity equation and the last two equations are the momentum equations respectively in r and z directions. We denote the derivatives by subscripts r and z where z denotes the distance along the axis of the glass tube and r measures the distance perpendicular to it. The velocity of the molten glass is defined to be $\bar{\mathbf{v}}=(u,v)$ where u and v are the components of velocity $\bar{\mathbf{v}}$ along z and r direction respectively. The pressure, density and the acceleration due to gravity are denoted by p,ρ and g respectively.

Now, at the free surfaces $r=r_1(z,t)$ and $r=r_2(z,t)$, it is necessary to specify the stress conditions and the kinematic conditions.

On the inner and outer surfaces of the glass tube, the stress conditions are given as:

$$\tau\hat{n}_i=-p_s\hat{n}_i \quad on \quad r=r_1,$$
$$\tau\hat{n}_o=0 \quad on \quad r=r_2,$$

where $\hat{n}_i$ and $\hat{n}_o$ are the unit normals on the surfaces $r=r_1$ and $r=r_2$ of the tube respectively defined as

$$\hat{n}_i=\frac{1}{\sqrt{1+\left(\frac{\partial r_1}{\partial z}\right)^2}}\left(1,-\frac{\partial r_1}{\partial z}\right) \quad \text{and}$$

$$\hat{n}_o=\frac{-1}{\sqrt{1+\left(\frac{\partial r_2}{\partial z}\right)^2}}\left(1,-\frac{\partial r_2}{\partial z}\right).$$

and p_s is the inside pressure applied on the surface $r=r_1$ of the glass tube.

The kinematic conditions are given by

$$v=\frac{\partial r_1}{\partial t}+\frac{\partial r_1}{\partial z}u \quad on \quad r=r_1, \tag{2.1d}$$

$$v=\frac{\partial r_2}{\partial t}+\frac{\partial r_2}{\partial z}u \quad on \quad r=r_2. \tag{2.1e}$$

The stress conditions can also be written as

$$-\mu\left(\frac{\partial v}{\partial z}+\frac{\partial u}{\partial r}\right)\frac{\partial r_1}{\partial z}+\left(-p+2\mu\frac{\partial v}{\partial r}\right)=-p_s \quad on \quad r=r_1, \tag{2.1f}$$

$$-\left(-p+2\mu\frac{\partial u}{\partial z}\right)\frac{\partial r_1}{\partial z}+\mu\left(\frac{\partial u}{\partial r}+\frac{\partial v}{\partial z}\right)=p_s\frac{\partial r_1}{\partial z} \quad on \quad r=r_1, \tag{2.1g}$$

$$\mu\left(\frac{\partial v}{\partial z}+\frac{\partial u}{\partial r}\right)\frac{\partial r_2}{\partial z}=-p+2\mu\frac{\partial v}{\partial r} \quad on \quad r=r_2, \tag{2.1h}$$

$$\left(-p+2\mu\frac{\partial u}{\partial z}\right)\frac{\partial r_2}{\partial z}=\mu\left(\frac{\partial u}{\partial r}+\frac{\partial v}{\partial z}\right) \quad on \quad r=r_2. \tag{2.1i}$$

The stress tensor τ reads as

$$\tau=\begin{pmatrix}-p+2\mu\frac{\partial v}{\partial r} & \mu\left(\frac{\partial u}{\partial r}+\frac{\partial v}{\partial z}\right)\\ \mu\left(\frac{\partial u}{\partial r}+\frac{\partial v}{\partial z}\right) & -p+2\mu\frac{\partial u}{\partial z}\end{pmatrix}$$

where μ denotes the viscosity of the molten glass which remains constant at the given temperature.

To take benefit of the small parameters present in the problem, it is now convenient to convert the Eqs. (2.1) into dimensionless form. For the dimensional quantities, the appropriate scaling is defined as:

$$z=L\tilde{z},\ r=\epsilon L\tilde{r},\ r_1=\epsilon L\tilde{r}_1,\ r_2=\epsilon L\tilde{r}_2,\ \mu=\mu_0\tilde{\mu},$$
$$u=U\tilde{u},\ v=\epsilon U\tilde{v},\ t=\tfrac{L}{U}\tilde{t},\ p=\tfrac{\mu_0 U}{L}\tilde{p},\ p_s=\tfrac{\mu_0 U}{L}\tilde{p}_s,$$

where $\epsilon=\frac{W}{L}\ll 1$. W is the width of the glass tube that has a very small value than the typical length of hot-forming zone L, U is the typical drawing speed and μ_0 is the typical melt glass viscosity which has a constant value for the isothermal case. After dropping the bar notation, the system of governing equations in dimensionless form is given as follows:

$$0=\frac{1}{r}\frac{\partial}{\partial r}(rv)+\frac{\partial u}{\partial z}, \tag{2.2a}$$

$$\frac{\partial p}{\partial r}=\mu\left(\frac{\partial^2 v}{\partial r^2}+\frac{1}{r}\frac{\partial v}{\partial r}-\frac{v}{r^2}\right)+\epsilon^2\frac{\partial}{\partial z}\left(\mu\frac{\partial v}{\partial z}\right)+\frac{\partial \mu}{\partial z}\frac{\partial u}{\partial r}+2\frac{\partial \mu}{\partial r}\frac{\partial v}{\partial r}, \tag{2.2b}$$

$$\epsilon^2\frac{\partial p}{\partial z}=\frac{1}{r}\frac{\partial}{\partial r}\left(\mu r\frac{\partial u}{\partial r}\right)+\epsilon^2\frac{\partial}{\partial z}\left(2\mu\frac{\partial u}{\partial z}\right)+\epsilon^2\frac{1}{r}\frac{\partial}{\partial r}\left(\mu r\frac{\partial v}{\partial z}\right)+\epsilon^2 St. \tag{2.2c}$$

The kinematics conditions (2.1d) and (2.1e) become

$$v=\frac{\partial r_1}{\partial t}+\frac{\partial r_1}{\partial z}u \quad on \quad r=r_1, \tag{2.2d}$$

$$v=\frac{\partial r_2}{\partial t}+\frac{\partial r_2}{\partial z}u \quad on \quad r=r_2. \tag{2.2e}$$

The stress conditions (2.1f)-(2.1i) read as

$$\left(-p+2\mu\frac{\partial v}{\partial r}\right)-\mu\left(\epsilon^2\frac{\partial v}{\partial z}+\frac{\partial u}{\partial r}\right)\frac{\partial r_1}{\partial z}=-p_s \quad on \quad r=r_1, \tag{2.2f}$$

$$\mu\left(\frac{\partial u}{\partial r}+\epsilon^2\frac{\partial v}{\partial z}\right)-\epsilon^2\left(-p+2\mu\frac{\partial u}{\partial z}\right)\frac{\partial r_1}{\partial z}=\epsilon^2 p_s\frac{\partial r_1}{\partial z} \quad on \quad r=r_1, \tag{2.2g}$$

$$-p+2\mu\frac{\partial v}{\partial r}=\mu\left(\epsilon^2\frac{\partial v}{\partial z}+\frac{\partial u}{\partial r}\right)\frac{\partial r_2}{\partial z} \quad on \quad r=r_2, \tag{2.2h}$$

$$\mu\left(\frac{\partial u}{\partial r}+\epsilon^2\frac{\partial v}{\partial z}\right)=\epsilon^2\left(-p+2\mu\frac{\partial u}{\partial z}\right)\frac{\partial r_2}{\partial z}\quad on\quad r=r_1. \tag{2.2i}$$

The above model can be simplified by means of an asymptotic expansion, in which the inverse aspect ratio ϵ is used as scaling parameter. Assuming the glass flow as a thin layer flow and ignoring the large aspect ratio of the flow, one derives the simplified equations to model the isothermal tube drawing process. In this derivation, the surface tension and inertial forces acting upon the molten glass have also been ignored due to their insignificant contributions. For details we refer to [1–4,32,33,38].

In view of the above considerations, the governing Eqs. (2.2) are reduced to the following model equations representing the isothermal process:

$$\frac{\partial A}{\partial t}+\frac{\partial}{\partial z}(vA)=0, \tag{2.3a}$$

$$\frac{\partial}{\partial z}\left(3\mu A\frac{\partial v}{\partial z}\right)+\rho gA=0, \tag{2.3b}$$

$$\frac{\partial}{\partial t}(R^2)+\frac{\partial}{\partial z}(vR^2)=\frac{p_s}{16\pi\mu A}\left(16\pi^2R^4-A^2\right), \tag{2.3c}$$

equipped with the initial conditions

$$A(z,0)=A_0,\ R(z,0)=R_0,\ \text{for } z\in[0,L], \tag{2.3d}$$

and the boundary conditions

$$A(0,t)=A_0,\ R(0,t)=R_0,\ v(0,t)=v_0,\quad v(L,t)=v_L,\ \text{for } t\geqslant 0, \tag{2.3e}$$

where A_0 and R_0 are the cross-sectional area and average radius of the glass tube at the time of entering the hot-forming zone, respectively. Acceleration due to gravity and density of the molten glass are denoted by g and ρ, respectively. Average radius R of the tube is defined as

$$R=\frac{1}{2}(r_1+r_2).$$

Equations in system (2.3) give us cross-sectional area A, velocity v, and average radius R of the glass tube. Width W of the tube can be determined by the equation

$$A=2\pi RW.$$

Since the temperature throughout the forming zone of the tubing process remains constant, the viscosity μ of the melt glass also remains constant.

2.1. Dimensionless form

In this subsection, we obtain dimensionless equations representing isothermal tube drawing model by introducing the following dimensionless quantities.

$$z^*=\frac{z}{L},\ t^*=\frac{v_0t}{L},\ A^*=\frac{A}{A_0},\ R^*=\frac{R}{R_0},\ v^*=\frac{v}{v_0},\ p^*=\frac{Lp_s}{\mu_0v_0},\ \text{and}\ \mu^*=\frac{\mu}{\mu_0}.$$

Using the above quantities into model (2.3), we obtain dimensionless equations given below:

$$\frac{\partial A}{\partial t}+\frac{\partial}{\partial z}(vA)=0, \tag{2.4a}$$

$$\frac{\partial}{\partial z}(3A\frac{\partial v}{\partial z})+StA=0, \tag{2.4b}$$

$$\frac{\partial}{\partial t}(R^2)+\frac{\partial}{\partial z}(vR^2)=\frac{\pi c_1p}{A}\left(R^4-\frac{A^2}{(4\pi c_1)^2}\right), \tag{2.4c}$$

where

$$St=\frac{\rho gL^2}{\mu v_0}\quad\text{and}\quad c_1=\frac{R_0^2}{A_0}, \tag{2.4d}$$

are the dimensionless parameters. Here St is known as Stokes number. We have avoided asterisks notations in above equations for the sake of simplicity. The initial and boundary conditions are transformed to following corresponding conditions:

$$A(z,0)=1,\ R(z,0)=1,\ \text{for all } z\in\Omega=[0,1], \tag{2.4e}$$

$$A(0,t)=1,\ R(0,t)=1,\ v(0,t)=1,\ v(1,t)=v_d,\ \text{for } t\geqslant 0, \tag{2.4f}$$

where $v_d=\frac{v_L}{v_0}>1$ is the draw ratio.

3. Steady-state model

The steady state form of the model (2.4) under the assumption that the state variables A, v, R are time t independent is given as follows:

$$\frac{d}{dz}(vA)=0, \tag{3.1a}$$

$$\frac{d}{dz}(3A\frac{dv}{dz})+StA=0, \tag{3.1b}$$

$$\frac{d}{dz}(vR^2)=\frac{\pi c_1p}{A}\left(R^4-\frac{A^2}{(4\pi c_1)^2}\right), \tag{3.1c}$$

subject to the conditions:

$$A(0)=1,\ v(0)=1,\ v(1)=v_d,\ R(0)=1. \tag{3.1d}$$

4. Existence and uniqueness

We now study the necessary conditions to obtain the existence and uniqueness of solution of steady state model (3.1). For the sake of simplicity, we ignore the constants and write the model (3.1) as:

$$\frac{d}{dz}(vA)=0, \tag{4.1a}$$

$$\frac{d}{dz}\left(A\frac{dv}{dz}\right)+A=0, \tag{4.1b}$$

$$\frac{d}{dz}(vR^2)-\frac{1}{A}\left(R^4-A^2\right)=0, \tag{4.1c}$$

$$A(0)=1,\ v(0)=1,\ v(1)=v_d,\ R(0)=1. \tag{4.1d}$$

Using (4.1d), an Eq. (4.1a) becomes

$$A(z)=\frac{1}{v(z)},\quad v(z)>0,\quad z\in\Omega. \tag{4.2}$$

Hence an Eq. (4.1b) can be written as

$$\frac{d^2}{dz^2}ln(v)=-v^{-1},\quad v(0)=1,\quad v(1)=v_d.$$

Using the transformation $w = ln(v)$, we obtain

$$-\frac{d^2w}{dz^2} - e^{-w} = 0, \qquad \text{on } \Omega,$$
$$w(0) = 0,$$
$$w(1) = ln(v_d).$$

To transform the boundary conditions into the homogeneous boundary conditions, we define a function on Ω as follows:

$$\gamma(z) = (ln(v_d))z, \quad \text{for } z \in \Omega.$$

Suppose that $\psi(z) = w(z) - \gamma(z)$. Thus, we have

$$-\frac{d^2\psi}{dz^2} - m(z)e^{-\psi} = 0, \qquad \text{on } \Omega = (0,1), \tag{4.3a}$$
$$\psi = 0 \qquad \text{on } \partial\Omega = \{0,1\}, \tag{4.3b}$$

where $m(z) = e^{-\gamma(z)} > 0$. The nonlinear variational problem corresponding to the Eq. (4.3) is defined as:

Find $\psi \in H_0^1(\Omega)$ such that

$$(\mathscr{A}\psi, \varphi) = 0, \qquad \text{forall } \varphi \in H_0^1(\Omega), \tag{4.4}$$

where the operator $\mathscr{A} : H_0^1(\Omega) \to H_0^1(\Omega)$ is defined by

$$(\mathscr{A}\psi, \varphi) = \int_\Omega \left(\frac{d\psi}{dz}\frac{d\varphi}{dz} - m(z)e^{-\psi}\varphi\right)dz, \ \varphi \in H_0^1(\Omega). \tag{4.5}$$

We need the following Lemmas to prove the existence and uniqueness of the solution of variation problem (4.4).

Lemma 4.1. *The operator $\mathscr{A} : H_0^1(\Omega) \to H_0^1(\Omega)$ defined by (4.5) is strongly monotone, that is, there exists a $\Theta > 0$ such that*

$$(\mathscr{A}\psi_1 - \mathscr{A}\psi_2, \psi_1 - \psi_2) \geqslant \Theta\|\psi_1 - \psi_2\|^2$$

holds for all $\psi_1, \psi_2 \in H_0^1$.

Proof: For $\psi_1, \psi_2 \in H_0^1(\Omega)$, we have

$$\begin{aligned}(\mathscr{A}\psi_1 - \mathscr{A}\psi_2, \psi_1 - \psi_2) &= \int_\Omega \left[\tfrac{d}{dz}(\psi_1 - \psi_2)\tfrac{d}{dz}(\psi_1 - \psi_2) - m(z)(e^{-\psi_1} - e^{-\psi_2})(\psi_1 - \psi_2)\right]dz \\ &\geqslant \int_\Omega \tfrac{d}{dz}(\psi_1 - \psi_2)\tfrac{d}{dz}(\psi_1 - \psi_2)dz \\ &= \int_\Omega \left|\tfrac{d}{dz}(\psi_1 - \psi_2)\right|^2 dz \\ &= \left\|\tfrac{d}{dz}(\psi_1 - \psi_2)\right\|^2 \\ &\geqslant \Theta\|\psi_1 - \psi_2\|^2,\end{aligned}$$

where $\Theta = \frac{1}{\mathbf{c}(\Omega)} > 0$, is a constant depending upon the domain of the problem. Hence the result. □

Lemma 4.2. *Function $\psi \in H_0^1(\Omega)$ used in* Eq. (4.3) *is positive for each z in its domain Ω.*

Proof: Note that $\psi(z) \neq 0$ for $z \in \Omega$. Indeed, it does not satisfy the Eq. (4.3a) otherwise. Let $\psi(z) < 0$ for $z \in \Omega$. The weak formulation of the Eq. (4.3) is given by

$$\int_\Omega \frac{d\psi}{dz}\frac{d\psi}{dz}dz - \int_\Omega m(z)e^{-\psi}\psi dz = 0, \text{ for } \psi \in H_0^1(\Omega) \text{ with } \psi < 0 \text{ in } \Omega,$$

or

$$\int_\Omega \left|\frac{d\psi}{dz}\right|^2 dz - \int_\Omega m(z)e^{-\psi}\psi dz = 0,$$

which is a contradiction. Indeed, both terms on the left hand side are strictly positive. Therefore, $\psi(z) > 0$ for $z \in \Omega$. □

Remark 4.3. For $0 < \psi_1, \psi_2 \in H_0^1$ the relation

$$|\, e^{-\psi_1} - e^{-\psi_2} \,| \leqslant \kappa \,|\, \psi_1 - \psi_2 \,|, \text{ for } \kappa > 0,$$

holds. We use the above remark in proving a crucial Lemma 4.4 stated below.

Lemma 4.4. *The operator $\mathscr{A} : H_0^1(\Omega) \to H_0^1(\Omega)$ defined by (4.5) is Lipschitz continuous, that is, there exists $\theta > 0$ such that*

$$\|\mathscr{A}\psi_1 - \mathscr{A}\psi_2\| \leqslant \theta\|\psi_1 - \psi_2\|,$$

for all $\psi_1, \psi_2 \in H_0^1(\Omega)$.

Proof: For any $\varphi \in H_0^1(\Omega)$, we obtain that

$$\begin{aligned}&|(\mathscr{A}\psi_1, \varphi) - (\mathscr{A}\psi_2, \varphi)| \\ &\leqslant \left|\int_\Omega \left(\frac{d}{dz}(\psi_1 - \psi_2)\frac{d\varphi}{dz}\right)dz\right| + \left|\int_\Omega m(z)(e^{-\psi_2} - e^{-\psi_1})\varphi dz\right| \\ &\leqslant \left\|\frac{d}{dz}(\psi_1 - \psi_2)\right\|_{L_2}\left\|\frac{d\varphi}{dz}\right\|_{L_2} + \kappa\|\psi_1 - \psi_2\|_{L_2}\|\varphi\|_{L_2}\|m\|_{L^\infty}, \\ &\leqslant \left\|\frac{d}{dz}(\psi_1 - \psi_2)\right\|_{L_2}\left\|\frac{d\varphi}{dz}\right\|_{L_2} + \kappa\mathbf{c}(\Omega)K\left\|\frac{d}{dz}(\psi_1 - \psi_2)\right\|_{L_2}\left\|\frac{d\varphi}{dz}\right\|_{L_2} \\ &= \theta\|\psi_1 - \psi_2\|_{H_0^1}\|\varphi\|_{H_0^1}, \ \theta = 1 + \kappa K\mathbf{c}(\Omega) > 0.\end{aligned}$$

Hence an operator $\mathscr{A}$ is a Lipschitz continuous. □

Lemma 4.5. [40] *Let $\mathbb{H}$ be a Hilbert space with scalar product $(.,.)$ and $B : \mathbb{H} \to \mathbb{H}$ a monotone and Lipschitz continuous operator. Then an operator equation*

$$B\psi = 0,$$

has a unique solution $\psi \in \mathbb{H}$.

Note that the solution obtained in the above Lemma is a fixed point φ of an auxiliary operator $T_r : \mathbb{H} \to \mathbb{H}$ defined by

$$T_r\varphi := \varphi - rB\varphi, \qquad \varphi \in \mathbb{H}.$$

Indeed, T_r is contractive operator provided that the parameter r lies in $(0, \frac{2\Theta}{L^2})$ where $\Theta > 0$ is a monotonicity constant and $\theta > 0$ is a Lipschitz constant.

Lemma 4.6. *An operator equation defined in (4.4) has a unique solution $\psi \in H_0^1(\Omega)$.*

Proof: By Lemmas 4.1 and 4.4, the operator $\mathscr{A}$ is strongly monotone and Lipschitz continuous. Therefore by the Lemma 4.5, there exists a unique solution to the Eq. (4.4). □.

Using Eq. (4.2), an Eq. (4.1c) takes the form

$$\frac{d}{dz}(vR^2) = A\left((vR^2)^2 - 1\right). \tag{4.6}$$

If we take $y(z) = v(z)R^2(z)$, then the Eq. (4.6) becomes

$$\frac{dy}{dz} = f(z, y, A), \quad \text{for } z \in \Omega \text{ with } y(z_0) = y_0, \tag{4.7}$$

where $f(z, y, A) = A(y^2 - 1), z_0 = 0, \text{ and } y_0 = 1.$

Theorem 4.7. [41] *Let the functions f and $\frac{\partial f}{\partial y}$ be continuous in some rectangle $\alpha < z < \beta, \sigma < y < \delta$ containing the point (z_0, y_0). Then, in some interval $z_0 - l < z < z_0 + l$ contained in $\alpha < z < \beta$, there is a unique solution $y = \eta(z)$ of the initial value problem,*

$$\frac{dy}{dz} = f(z,y), \quad y(z_0) = y_0. \quad \square$$

Lemma 4.8. *Let A and y be continuous functions of z. If the functions f and $\frac{\partial f}{\partial y}$ are continuous in some rectangle $\alpha < z < \beta$, $\sigma < y < \delta$ containing the point (z_0, y_0), then there exists a unique solution $y(z)$ to the initial value problem (4.7) in some neighborhood of (z_0, y_0).*

Proof: Obviously

$$f = A(y^2 - 1) \quad \text{and} \quad \frac{\partial f}{\partial y} = 2yA, \tag{4.8}$$

are continuous functions of z. It follows from Theorem 4.7 that there exists a unique solution to the Eq. (4.7) in some neighborhood of (z_0, y_0). $\square$

Remark 4.9. Existence and uniqueness of the solutions of the differential Eq. (4.1a) follows from the Lemma 4.6 and Eq. (4.2).

5. Solution strategy of steady-state model

In view of (4.2), the model (3.1) is now reduced to

$$\frac{d^2v}{dz^2} = \frac{1}{v}\left(\frac{dv}{dz}\right)^2 - \frac{St}{3}, \tag{5.1a}$$

$$\frac{dR}{dz} = -\frac{R}{2v}\frac{dv}{dz} + \frac{\pi c_1 p}{2R}\left(R^4 - \frac{1}{(4\pi c_1 v)^2}\right), \tag{5.1b}$$

with following conditions

$$v(0) = 1, \; v(1) = v_d, \; R(0) = 1. \tag{5.1c}$$

For numerical solution of (5.1), we use shooting method along with MATLAB ODE solver *ode45*.

5.1. Shooting method

Shooting method [43] transforms the boundary value problem (BVP) into a set of initial value problems (IVPs) that can be solved using existed ODE solvers. Let

$$\frac{dv}{dz} = \Psi.$$

The model (5.1) can be written as:

$$\frac{dv}{dz} = \Psi, \tag{5.2a}$$

$$\frac{d\Psi}{dz} = \frac{\Psi^2}{v} - \frac{1}{3}St, \tag{5.2b}$$

$$\frac{dR}{dz} = -\frac{R}{2v}\frac{dv}{dz} + \frac{\pi c_1 p}{2R}\left(R^4 - \frac{1}{(4\pi c_1 v)^2}\right), \tag{5.2c}$$

with conditions:

$$v(0) = 1, \; v(1) = v_d, \; R(0) = 1. \tag{5.2d}$$

For sake of simplicity, we now put the model (5.2) into a compact form

$$\frac{dV}{dz} = F(V,z), \forall\, z \in \Omega, \text{ with } V_1(0) = 1, \; V_1(1) = v_d, \; V_3(0) = 1, \tag{5.3}$$

where $V = [v(z), \Psi(z), R(z)]^T \in \mathbb{R}^3$.

Thus the corresponding IVP is given as

$$\frac{dV}{dz} = F(V,z), \forall\, z \in \Omega, \text{ with } V_1(0) = 1, \; V_2(0) = s, \; V_3(0) = 1, \tag{5.4}$$

where the initial guess s is to be chosen such that V_1 hits v_d at $z = 1$.

The role of a parameter s is very crucial and hence we denote the solution of IVP (5.4) by $V(z,s)$. If we can compute a value of s such that

$$E(s) = V(1,s) - v_d = 0, \tag{5.5}$$

then the solution of the IVP (5.4) coincides with the solution of the BVP (5.3). We approximate the root of the Eq. (5.5) using the Newton–Raphson method. To achieve this, we proceed as follows: Let E be differentiable function over $(0,1)$ such that $\frac{dE}{ds} \neq 0$ and $E(0)E(1) < 0$, and hence there exists at least one number $\bar{s} \in (0,1)$ such that $E(\bar{s}) = 0$. The sequence $\{s_n\}_{n\in N}$ generated by the Newton Raphson method given as follows:

$$s_{i+1} = s_i - \frac{E(s_i)}{E'(s_i)}, \quad i = 0, 1, 2, \ldots \tag{5.6}$$

which converges to $\bar{s}$ for some suitable initial guess s_0. The suitable guess s_0 is attained by performing a few iterations of the bisection method. To implement bisection method, we consider two initial guesses s_0^1 and s_0^2 with $s_0^1 < s_0^2$ such that

$$E(s_0^1)E(s_0^2) < 0. \tag{5.7}$$

This guarantees the existence of at least one $\bar{s} \in [s_0^1, s_0^2]$ such that $E(\bar{s}) = 0$; a root of an Eq. (5.5). Next, we find the mid point s_0^3 of interval $[s_0^1, s_0^2]$ and determine the sign of $E(s_0^3)$. If $E(s_0^3)E(s_0^2) < 0$, then the Eq. (5.5) has a root over the interval $[s_0^3, s_0^2]$, otherwise the root exists in $[s_0^1, s_0^3]$. This process is repeated to obtain a sequence $\{s_n\}_{n\in N}$ which converges to $\bar{s}$. Since this convergence is very slow, we stop bisection iterations when the length of the last interval containing the root is less than the given tolerance. The mid point of the last interval gives the best initial guess s_0 for the Newton's iterations (5.6). To implement Newtons's iterations (5.6), we also need $E'(s_n)$. For this, we define $\Phi(z,s)$ as follows:

$$\Phi(z,s) = \left.\frac{\partial V}{\partial s}\right|_{z=1} = E'(s), \tag{5.8}$$

and formulate a second initial value problem as follows

$$\frac{\partial \Phi}{\partial z} = \left(\frac{\partial F}{\partial V}\right)\Phi \quad \text{with } \Phi_1(0,s) = 0, \; \Phi_2(0,s) = 1, \; \Phi_3(0,s) = 0. \tag{5.9}$$

We solve the initial value problems (5.4) and (5.9) for $V_1(1,s_0)$ and $\Phi_1(1,s_0)$ which respectively give us $E(s_0)$ (by (5.5)) and $E'(s_0)$. Now Newton's iterations (5.6) give the next refined guess s_{i+1}, $i = 0, 1, \ldots$. The process is repeated until we obtain the result. The numerical strategy given above is implemented through the following algorithm.

Algorithm 1.

(1) Make two initial guesses s_0^1 and s_0^2 such that $s_0^1 < s_0^2$ for $V_2(0)$.
(2) Solve (5.4) for each of the guess and then solve (5.5) for $E(s_0^1)$ and $E(s_0^2)$.
(3) If $E(s_0^1)E(s_0^2) > 0$ move to step 1 otherwise move to next step.
(4) Find $s_0^3 = \frac{s_0^1+s_0^2}{2}$, if $E(s_0^2)E(s_0^3) < 0$, set $s_0^1 = s_0^3$, otherwise $s_0^2 = s_0^3$.
(5) If $| s_0^1 - s_0^2 | > tol_1$, move to step 4 otherwise $s_0 = \frac{s_0^1+s_0^2}{2}$.
(6) Evaluate the initial value systems (5.4) and (5.9).
(7) If $| E(s_i) | > tol_2$, find s_{i+1} using (5.6) and move to step 6 otherwise STOP.

Here tol_1 and tol_2 are set to terminate the computing process.

The parametric values appearing in the model (3.1) are given in the Table 1.

6. Linear stability analysis

In this section, we investigate the stability of tube drawing process employing a linear stability analysis. We construct an eigenvalue problem and solve it to determine the critical draw ratio to investigate the stability of the model. To achieve this goal, we re-write the equations of the isothermal model (2.4) in the form

$$\frac{\partial A}{\partial t} = -A\frac{\partial v}{\partial z} - v\frac{\partial A}{\partial z}, \tag{6.1a}$$

$$0 = A\frac{\partial^2 v}{\partial z^2} + \frac{\partial A}{\partial z}\frac{\partial v}{\partial z} + \frac{1}{3}StA, \tag{6.1b}$$

$$\frac{\partial R^2}{\partial t} = -v\frac{\partial R^2}{\partial z} - R^2\frac{\partial v}{\partial z} + \frac{\pi c_1 p R^4}{A} - \frac{\pi c_1 p A}{(4\pi c_1)^2}, \tag{6.1c}$$

along with the initial and boundary conditions given by (2.4e) and (2.4f).

To determine the linear stability, the first step is to linearize the system (6.1). For this purpose, we split the unsteady solution $v(z,t), A(z,t)$ and $R(z,t)$ into the form given as

Table 1 Summary of parametric values appearing in the model (3.1).

Parameters	Symbols	Approximate Values	Units
feeding speed	v_0	1	mm/s
drawing speed	v_L	12	mm/s
length of the hot-forming zone	L	1	m
viscosity	μ_0	5×10^5	Pa.s
inside pressure	p_s	420	Pa
density	ρ	2500	kg/m^3
average radius of the glass tube	R_0	30	mm
initial area of the tube	A_0	1885	mm

$$v(z,t) = v_s(z) + \Lambda(z)e^{\lambda t}, \tag{6.2a}$$

$$A(z,t) = A_s(z) + \phi(z)e^{\lambda t}, \tag{6.2b}$$

$$R(z,t) = R_s(z) + \varrho(z)e^{\lambda t}, \tag{6.2c}$$

where $\Lambda(z), \phi(z), \varrho(z)$ are the perturbed quantities of the state variables $A(z,t), v(z,t), R(z,t)$ respectively; $\lambda \in \mathbb{C}$, a complex eigenvalue which determines the rate of growth of the perturbations $\Lambda(z)$, $\phi(z), \varrho(z)$, and v_s, A_s, R_s denote the steady-state solutions of model (3.1), respectively.

6.1. Eigenvalue equations

We Substitute the Eqs. (6.2) into system (6.1) and ignore the higher order terms to obtain the following linearized system for the isothermal flow.

$$\Omega\phi = a_1\phi + a_2\frac{d\phi}{dz} + a_3\Lambda + a_4\frac{d\Lambda}{dz}, \tag{6.3a}$$

$$0 = b_1\phi + b_2\frac{d\phi}{dz} + b_3\frac{d\Lambda}{dz} + b_4\frac{d^2\Lambda}{dz^2}, \tag{6.3b}$$

$$\Omega\varrho = d_1\phi + d_2\Lambda + d_3\frac{d\Lambda}{dz} + d_4\varrho + d_5\frac{d\varrho}{dz}, \tag{6.3c}$$

subject to the boundary conditions given by

$$\Lambda(0) = 0,\ \Lambda(1) = 0,\ \phi(0) = 0,\ \varrho(0) = 0, \tag{6.3d}$$

where a_i, b_i and d_i are functions of z and read as

$$\begin{aligned}
a_1 &= -v_s', & a_2 &= -v_s,\\
a_3 &= \tfrac{v_s'}{v_s^2}, & a_4 &= -\tfrac{1}{v_s},\\
b_1 &= v_s'' + \tfrac{1}{3}St, & b_2 &= v_s',\\
b_3 &= -\tfrac{v_s'}{v_s^2}, & b_4 &= \tfrac{1}{v_s},\\
d_1 &= -v_s^2R_s' - K_2\tfrac{1}{R_s} - \tfrac{1}{2}v_sv_s'R_s, & d_2 &= -R_s',\\
d_3 &= -\tfrac{1}{2}R_s, & d_4 &= -v_s' - v_s\tfrac{R_s'}{R_s} + 2K_1v_sR_s^2,\\
d_5 &= -v_s.
\end{aligned}$$

Here $K_1 = \pi c_1 p$ and $K_2 = \frac{\pi c_1 p}{(4\pi c_1)^2}$.

6.2. Numerical solution

We discretize the linearized system (6.3) using finite difference approximations on an equally spaced grid $z_i = ih, i = 0, 1, 2, \ldots, n$ with grid size $h = \frac{1}{n}$. The derivatives are approximated as follows:

$$\frac{d\xi}{dz}(z_i) \approx \frac{\xi_{i+1}-\xi_{i-1}}{2h},$$
$$\frac{d^2\xi}{dz^2}(z_i) \approx \frac{\xi_{i+1}-2\xi_i+\xi_{i-1}}{h^2},$$

where $\xi_i = \xi(z_i)$ and $i = 1, 2, \ldots, n-1$. We apply the backward difference approximations to obtain

$$\frac{d\xi}{dz}(z_i) \approx \frac{\xi_i-\xi_{i-1}}{h},$$
$$\frac{d^2\xi}{dz^2}(z_i) \approx \frac{\xi_i-2\xi_{i-1}+\xi_{i-2}}{h^2},$$

for the end point $i = n$.

We have three unknowns Λ_i, ϕ_i and ϱ_i at each grid point z_i. Finite difference approximations of derivatives are plugged into the system (6.3) and the terms are re-arranged to get the following system of discretized equations (eigenvalue equations)

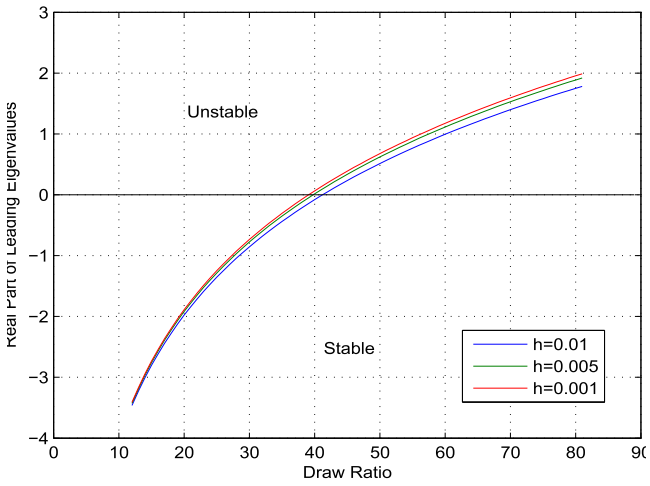

Fig. 3 Plot of real part of the leading eigenvalues against the draw ratio $v_d = \frac{v_L}{v_0} > 1$ for the density $\rho = 2500$.

$$M\phi + N\Lambda - \lambda\phi = 0, \tag{6.5a}$$
$$X\phi + Y\Lambda = 0, \tag{6.5b}$$
$$S\phi + T\Lambda + U\varrho - \lambda\varrho = 0, \tag{6.5c}$$

where M, N, X, Y, S, T and U are coefficient matrices. Eq. (6.5b) leads us to

$$\Lambda = -Y^{-1}X\phi,$$

provided that the matrix Y is invertible. Now substituting Λ into matrix Eqs. (6.5a) and (6.5c), we obtain the system

$$Q_{11}\phi - \lambda\phi = 0,$$
$$Q_{21}\phi + Q_{22}\varrho - \lambda\varrho = 0.$$

In a compact form, we have

$$Q\xi = \lambda\xi, \tag{6.7}$$

where

$$Q = \begin{pmatrix} Q_{11} & O \\ Q_{21} & Q_{22} \end{pmatrix}, \quad \xi = \begin{pmatrix} \phi \\ \varrho \end{pmatrix},$$

and

$$Q_{11} = M - NY^{-1}X,$$
$$Q_{21} = S - TY^{-1}X,$$
$$Q_{22} = U.$$

are the block matrices. To determine the linear stability of the isothermal tube drawing model (2.4), we find the eigenvalues λ_i of the eigenvalue problem (6.7) and check the sign of their real parts. If real part of λ_i is positive, that is, $Re(\lambda_i) > 0$ for any i, then the given system is unstable which indicates the unbounded growth of the state variables with time. The system will be stable only if each eigenvalue λ_i has negative real part. We are unable to determine the behavior of the physical system if we do not have any of the above said situations. The minimal value of the draw ratio where instability occurs is called critical draw ratio denoted by d_c. To determine critical draw ratios of isothermal tube drawing, we plug the numerical solution A_s, v_s, and R_s of steady state model (3.1) into the eigenvalue problem (6.7) and solve it for the eigenvalues of the matrix Q. Stability of the model is discussed on the basis of computed eigenvalues/critcal draw ratios.

6.3. Numerical implementations of results

In Fig. 3, real parts of the leading eigenvalues have been plotted against draw ratios for three different step sizes $h = 0.01, 0.005$ and 0.001. A plot of critical draw ratios against three step sizes is shown in Fig. 4 and the corresponding data is given in the Table 2. We observe a small decrease in the critical draw ratio for the drawing process with the decrease in the step size h. This shows that step size h has a minor influence on the process stability. Stable and unstable regions are also shown in both of these figures. For further analysis, we investigate the effect of density ρ, viscosity μ and the pressure p_s on the critical

Table 2 Critical draw ratios for different values of h.

Step size	$h = 0.01$	$h = 0.005$	$h = 0.001$
Critical draw ratio	41.215	39.919	38.882

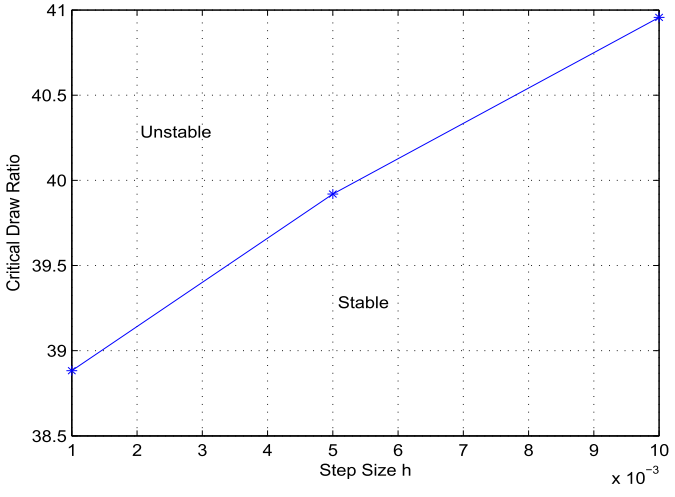

Fig. 4 Plot of critical draw ratio d_c against the step size $h = 0.01, 0.005, 0.001$.

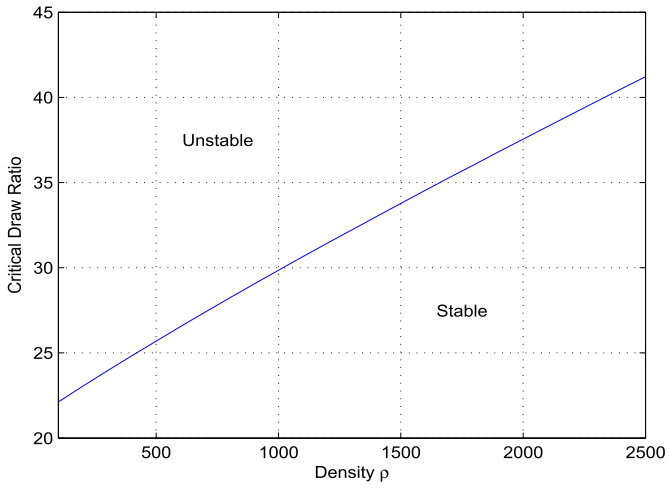

Fig. 5 Critical draw ratio d_c against the density ρ where $h = 0.01$.

draw ratio d_c. Fig. 5 shows that critical draw ratio changes linearly with increase in density of the material. The stable and unstable regions are also shown in this figure. Table 3 gives the numerical view of the Fig. 5. The critical draw ratio increases with the increase in density of the melt glass, by which the onset of instability is shifted to higher critical draw ratios. Thus, by setting higher density of melt glass, the stability of the isothermal tube drawing process can be improved. On the other hand, the critical draw ratio decreases with the increase in viscosity of molten glass as illustrated in Table 4. The stable and unstable regions are shown in Fig. 6. This decrease in critical draw ratio will regress the stability of the

Table 3 Critical draw ratio for the isothermal case depending on density of molten glass with step size $h = 0.01$

Critical draw ratio	Density
22.125	100
25.695	500
29.855	1000
33.775	1500
37.545	2000
41.215	2500

Table 4 Critical draw ratio for the isothermal case depending on viscosity of molten glass with step size $h = 0.01$ and $\rho = 2500$.

Critical draw ratio	Viscosity
41.215	5.0×10^5
39.565	5.5×10^5
38.165	6.0×10^5
36.975	6.5×10^5
35.945	7.0×10^5
35.045	7.5×10^5

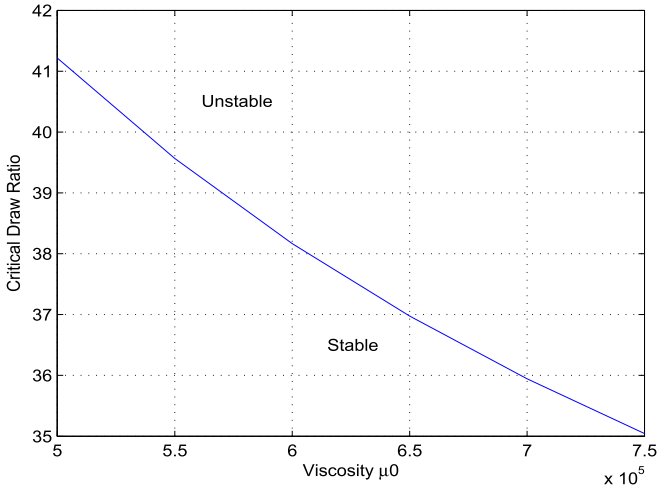

Fig. 6 Critical draw ratio d_c against the viscosity μ_0 where $h = 0.01$.

isothermal tube drawing process. Moreover, it is observed that stability of the isothermal tube drawing process with respect to pressure p_s does not change. The obtained stable/unstable regions in practice can influence the tube drawing process. Practically, stable region gives the reliability of the process with respect to the parameters involved over which the manufacturing process works well and fulfills all the desired properties of the tube drawn. On the other hand, the unstable region is the region where minimal value of the draw ratio disappears. As a result, the tubing process behaves unstable and do not work well. We discuss all of the numerical results with stable and unstable regions.

7. Conclusions

The main purpose of this study is to analyze the isothermal tube drawing process with respect to some process parameters, which can be unstable by such parameters when some critical conditions are exceeded. That's why, stability of the tube

drawing process with respect to process parameters is important in glass industry. To analyze the isothermal tubing process, linear stability method (a typical stability tool) has been used. We formulated an eigenvalue problem and solved it using MATLAB ODE solver *ode*45 and the MATLAB routine *eig*.

For the parametric values given in Table 1 and for $h = 0.01$, the critical draw ratio for isothermal tube drawing process is noticed to be 41.215. We also noticed that there is a small change in the critical draw ratio d_c with the change in step size h. With the refinement of the step size, we have a minor decrease in the critical draw ratio. So, the stability of tube drawing process is influenced negligibly by a step size h.

We further analyzed the stability of isothermal tube drawing process with respect to the material properties such as density and viscosity etc. We observed that the critical draw ratio increases linearly with the increase in the density of the molten glass. Hence, the stability of the isothermal tube drawing process can be improved by taking higher density of the material. We also study the effect of viscosity on the stability of the process. It is observed that increase in viscosity of the material gives the small regress in stability of the model. For the isothermal process, we noticed that stability domain of the model is independent of the air pressure.

Declaration of Competing Interest

The authors declare that they have no known competing financial interests or personal relationships that could have appeared to influence the work reported in this paper.

References

[1] A.I.K. Butt, Optimal control of tube drawing processes PhD thesis, Technische Universitat Kaiserslauten, Germany, 2009.

[2] A.I.K. Butt, R. Pinnau, Optimal control of a non-isothermal tube drawing process, J. Eng. Mathe. 76 (2012) 1–17.

[3] A.D. Fitt, K. Furusawa, T.M. Monro, C.P. Please, D.J. Richardson, The mathematical modelling of capillary drawing for holey fiber manufacture, J. Eng. Math. 43 (2002) 201–227.

[4] I.M. Griffiths, P.D. Howell, Mathematical modeling of non-axisymmetric capillary tube drawing, J. Fluid Mech. 605 (2008) 181–206.

[5] T. Bernard, E.E. Moghaddam, Nonlinear model predictive control of a glass forming process based in a finite element model, in: IEEE International Conference on Control Applications, Munich, Germany 2006; Conference Proceedings, pp. 960–965.

[6] G. Murad, I. Postlethwaite, D.-W. Gu, J.F. Whidborne, Robust Control of a Glass Tube Production Process, IEE, Syvoy Place, London UK, 1994.

[7] Sang-Kon Lee, Myeong-Sik Jeong, Byung-Min Kim, Seong-Kon Lee, Seon-Bong Lee, Die shape design of tube drawing process using FE analysis and optimization method, Int. J. Adv. Manuf. Technol. 66 (2013) 381–392.

[8] Nima Dabiri Farahani, Ali Parvizi, Ali Barooni and Sina Anvari Naeini, Optimum curved die profile for tube drawing process with fixed conical plug, Int. J. Adv. Manuf. Technol. 97 (2018) 1–11 .

[9] M. Hinze, R. Pinnau, An optimal control approach to semiconductor design, Math. Models Methods Appl. Sci. 12 (2002) 89–107.

[10] M. Hinze, R. Pinnau, Second-order approach to optimal semiconductor design, J. Optim. Theory Appl. 133 (2007) 179–199.

[11] M. Hinze, R. Pinnau, Mathematical tools in optimal semiconductor design, Bull. Inst. Math. Acad. Sin. (New Series) 2 (2) (2007) 569–586.

[12] M. Hinze, R. Pinnau, M. Ulbrich, S. Ulbrich, Optimization with PDE Constraints, Springer, 2009.

[13] M. Hinze, S. Volkwein, Instantaneous control for the instationary burgers equation-convergence analysis and numerical implementations, Nonlinear Anal., Theory, Methods Appl. 50 (2002) 1–26.

[14] R. Pinnau, G. Thommes, Optimal boundary control of glass cooling processes, Mathe. Methods App. Sci. 27 (2004) 1261–1281.

[15] K. Selvanayagam, T. Gotz, S. Sundar, V. Vetrivel, Optimal control of film casting processes, Int. J. Num. Math. Fluids (2008).

[16] A. Schulze, Minimizing Thermal Stress in Glass Production Processes: Model Reduction and Optimal Control. PhD thesis. TU Kaiserslautern, 2007.

[17] Christoph Hartl, Review on advances in metal micro-tube forming, Metals 9 (2019) 542, https://doi.org/10.3390/met9050542.

[18] Praveen Kumar, Dr. Geeta Agnihotri, Cold Drawing Process-A Review, International Journal of Engineering Research and Applications (IJERA) ISSN: 2248–9622 www.ijera.com, Vol. 3, Issue 3, May-Jun 2013, pp. 988–994.

[19] Heinz Palkowski, Sebastian Bruck, Thilo Pirling, Adele Carrado, Investigation on the Residual Stress State of Drawn Tubes by Numerical Simulation and Neutron Diffraction Analysis, ISSN 1996-1944 www.mdpi.com/journal/materials, Mate.rials (2013), 6, 5118-5130; doi:10.3390/ma6115118.

[20] P. Bella1, P Bucek, Numerical simulation of multi-rifled tube drawing-finding proper feedstock dimensions and tool geometry, in: 4th International Conference Recent Trends in Structural Materials, IOP Conf. Series: Materials Science and Engineering 179 (2017) 012008 doi:10.1088/1757-899X/179/1/012008

[21] D. Gelder, The stability of fiber drawing processes, Ind. Eng. Chem. Fund. 10 (1971) 534–543.

[22] R.J. Fisher, M.M. Denn, A theory of isothermal melt spinning and draw resonance, AIChE J. 22 (1976) 236–246.

[23] H.W. Jung, H.S. Song, J.C. Hyun, Draw resonance and kinematic waves in viscoelastic isothermal spinning, AIChE J. 46 (10) (2000) 2106–2110.

[24] J.S. Lee, H.W. Jung, J.C. Hyun, L.E. Seriven, Simple indicator of draw resonance instability in melt spinning processes, AIChE J. 51 (10) (2005) 2869–2874.

[25] T. Hagen, Eigenvalue asymptotics in isothermal forced elogation, J. Mathe. Anal. Appl. 244 (2000) 393–407.

[26] M. Renardy, Draw resonance revisited, SIAM J. Appl. Mathe. 66 (2006) 1261–1269.

[27] D.M. Shin, J.S. Lee, H.W. Jung, J.C. Hyum, High speed fiber spinning process with spinline flow-induced crystallization and neck-like deformation, Rheol. Acta 45 (2006) 575–582.

[28] B. Suman, P. Tandon, Fluid flow stability analysis of multilayer fiber drawing, Chem. Eng. Sci. 65 (2010) 5537–5549.

[29] R. Van der Hout, Draw Resonance in isothermal fiber spinning of newtonian and power-law fluids, Eur. J. Appl. Mathe. 11 (2000) 129–136.

[30] T. Götz, S.S.N. Perera, Stability ananlysis of the melt spinning process with respect to parameters, ZAMM-J. Appl. Mathe. Mech. 89 (2009) 874–880.

[31] S.S.N. Perera, Analysis and optimal control of melt spinning process PhD thesis, University of Colombo, Srilanka, 2008.

[32] A.D. Fitt, K. Furusawa, T.M. Monro, C.P. Please, Modelling the fabrication of hollow fibers: capillary drawing, J. lightwave Technol. 19(12) (2001).
[33] D. Krause, H. Loch (Eds.) Mathematical Simulation in Glass Technology, Springer-Verlag, Berlin, Heidelberg, 2002, pp. 293–307.
[34] L.J. Cummings, P.D. Howell, On the evolution of non-axisymmetric viscous fibers with surface tension, inertia and gravity, J. Fluid Mech. 389 (1999) 361–389.
[35] S.D. Sarboh, S.A. Milinkovic, D.L.J. Debeljkovic, Mathematical model of the glass capillary tube drawing process, Glass Technol. 39 (1998) 53–67.
[36] S.H.-K. Lee, Y. Jaluria, Simulation of the transport process in the neck-down region of a furnace drawn optical fiber, Int. J. Heat Mass Transfer 40 (1997) 843–856.
[37] U.B. Paek, R.B. Runk, Physical behaviour of the neck-down region during furnace drawing of silica fibers, J. App. Phys. 40 (1978) 4417–4422.
[38] P.D. Howell, Extensional Thin Layer Flows PhD thesis, St. Catherine's College, Oxford, 1994.
[39] M. Palengat, O. Guiraud, C.Millet, G. Chagnon, D. Favier Tube Drawing Process Modelling By A Finite Element Analysis, 2007, DOI: 10.1063/1.2740893.
[40] Christian Grossmann, Hans-Grg Roos, Martin Stynes, Numerical Treatment of Partial Differential Equations, Springer-Verlag, Berlin Heidelberg, 2007.
[41] William E. Boyce, Richard C. Diprima, Elementary Differential Equations, 6th ed., John Wiley and Sons, Inc., 1997.
[42] A.I.K. Butt, K Mumtaz, E Resendiz-Flores, Space mapping for optimal control of a non-isothermal tube drawing process., Math Meth Appl Sci.2020;1-12 of Engg. (2020) 1–12, https://doi.org/10.1002/mma.6395.
[43] Keller, H.B., Numerical methods for two-point boundary value problems, SIAM, Philadelphia (1976).